Proceedings World Geothermal Congress 2010
Bali, Indonesia, 25-29 April 2010

Design and Analysis of Low Temperature Field Tracer Test Case Study

Tevfik Kaya[a], Serhat Akin[a], Mahmut Parlaktuna[a]

[a]Petroleum & Natural Gas Engineering Department Middle East Technical University 06531 Ankara – Turkey

tevfik.kaya@superonline.com, serhat@metu.edu.tr, mahmut@metu.edu.tr,

Keywords: Geothermal, Tracer, Low Temperature, Kizilcahamam

ABSTRACT

Kizilcahamam is a low temperature (~ 80°C) geothermal field located 70 km from Ankara, Turkey. The produced geothermal water is used to heat more than 2500 houses. In order to characterize the reservoir, a tracer-test was planned using the efficient hydrologic tracer-test design technique. The test was carried out by injecting a slug of fluorescein into a shallow re-injection well. Analysis of the results showed that the injection well and the producers are interconnected. Analysis of time-concentration curves showed that a multi-fracture model represented the multi-peaked curves better than the others, which included homogeneous porous and double porosity models. The results are consistent with the conceptual geological models proposed in the literature.

1. INTRODUCTION

The Kızılcahamam geothermal field is located 70 km from Ankara, as shown in Figure 1. The geothermal fluid, produced with an average temperature of 74–86°C (Gevrek, I, 2000) and a flowrate of 80 l/s is used in the district heating of 2500 houses, in thermal hotels (Başkent University Thermal Hotel, Asya Thermal Resorts, Ab-ı Hayat and municipality hotels), and in district facilities by using heat exchangers (Kaya, 2005). Used geothermal water is reinjected to the reservoir at a flowrate of 40 l/s and a temperature of approximately 42°C into a shallow reinjection well and a deep reinjection well. A total of 6 production and 2 reinjection wells are currently present in the field, as illustrated in Figure 2. The deep reinjection well (KHD-1) is used as a production well during winters. All production wells use pumps at depths between 50 and 66 meters, as displayed in Table 1.

The objective of this study is to characterize and describe a tracer test conducted recently. In this paper, the geology and current situation of the field is described, followed by the tracer test design and its evaluation.

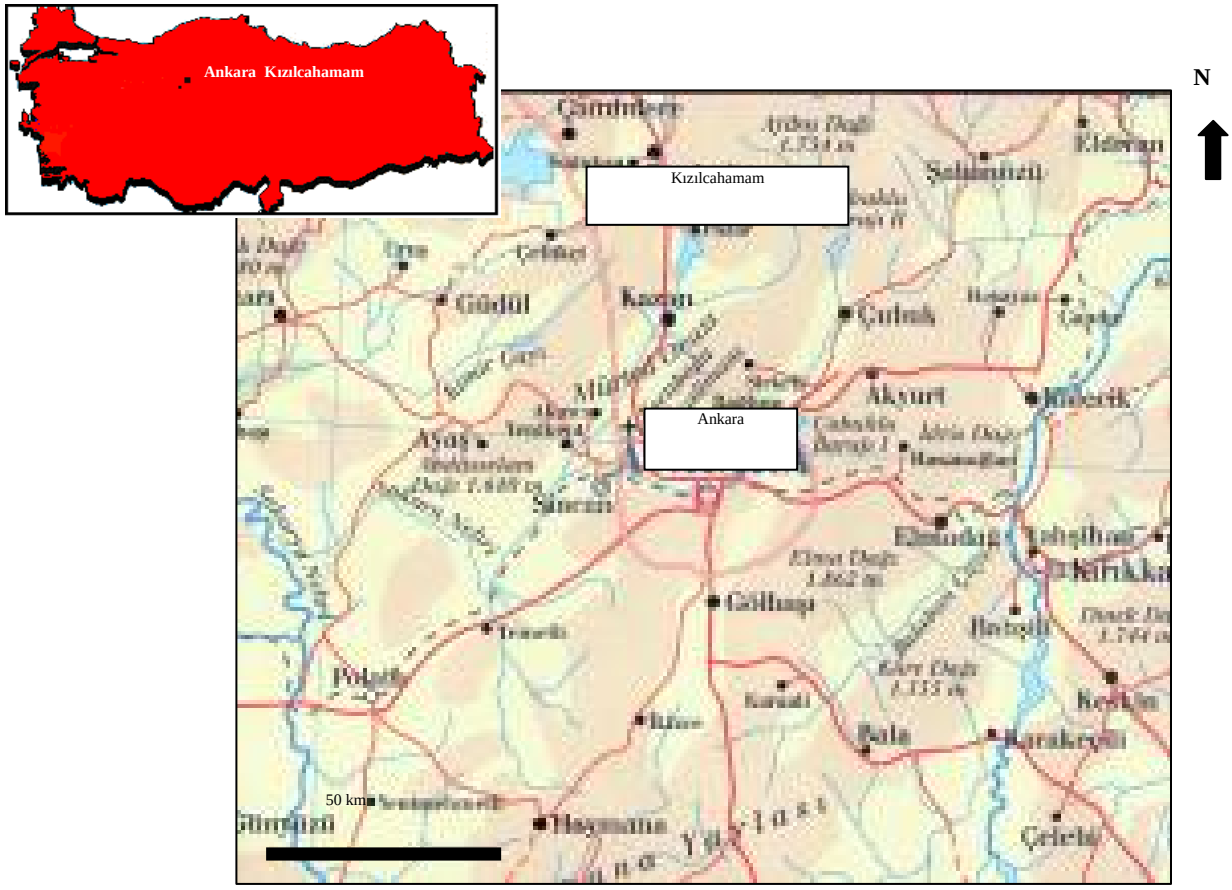

.

Figure 1: Map showing the location of the Kizilcahamam geothermal field

Table 1: Production and injection well properties

Name of the Well	Well Depth (m)	Flow rate (l/s)	Well head temperature (°C)	Dynamic Level (m)	Pump depth (m)
MTA-1(re-injection)	179	40	42	0	0
MTA-2	310	30	76	120	65
KHD-1(re-injection)	1556	15	42	0	0
İHL-1	590	20	76	25	65
İHL-2	670	40	74	30	66
İHL-3	673	20	79	20	57
FETHIBEY	592	20	76	25	65
Asya Finans	600	20	65	25	50

2.1 Geology

Geological, geochemical and geophysical studies have been carried out in this area by Tatli (1975), Ongur (1976), Kocak (1977), Demirorer (1985), Gurer and Celik (1987), Gevrek and Aydin (1988), Ozbek (1988) and Gulec (1994). The Kızılcahamam area is located within the Tertiary-aged Galatian Volcanic Province that consists of autoclastic and pyroclastic deposits (Gevrek, 2000).

Stratigraphic units (approximately 1800 m) from the bottom to the top are as follows:

1. Basaltic lava flows (Paleocene) 2. Pyroclastic deposits consisting of tuffs and agglomerates (Miocene); 3. Undifferentiated lava flows ranging in composition from andesitic, basaltic, trachyandesitic to dacitic (Miocene); 4. Debris flows (Quaternary). All of the units of the KHD-1 stratigraphic column are illustrated in Figure 4.

The basement beneath the province consists of Paleozoic schists and Permo-Triassic limestones. The Lower Cretaceous limestone and Upper flysch facies and limestone lie over the Paleozoic basement, and are overlain by the Galatian Volcanic Province.

The volcanic activity is believed to have started at the end of the Upper Cretaceous and reached its climax during the Miocene age (Gevrek, 2000). Gravity faults, which strike dominantly in the ENE–WSW direction, have been observed in the district. The Kızılcahamam fault, which passes through the town, has approximately an E–W direction and is 2250 m in length. A diagram of the Kizilcahamam geothermal system is given in Figure 3.

1.2 Chemical properties of geothermal fluid

Thermal waters issuing through the Tertiary aged volcanics in the Kizilcahamam geothermal area are all alkali-bicarbonate waters with temperatures ranging from 28°C to 86°C. The waters from the town center have the highest temperature and an intermediate total dissolved solid content compared to the waters sampled in the localities outside the town center.

The Kızılcahamam geothermal water has a pH of approximately 7.2. It contains bicarbonate, chlorite, sodium, carbon dioxide and arsenic.

The water is suitable for balneology, and Kızılcahamam thermal water has a solution mineral value of 250 mg/l. The chemical classification is as follows: bicarbonate (67.18%), chlorite (19.22%), sodium (82.64%), arsenic (0.34 mg/l) and carbon dioxide (283.4 mg/l). Metaboric acid (18.95 mg/l) and fluorite (1.96 mg/l) are also present (Kaya, 2005).

The variations in the temperature and the chemical composition of the waters can be accounted for by a combination of processes including mixing between cold-shallow and hot-deep waters, boiling either before or after mixing, steam heating and conductive cooling.

The chemical geothermometers, silica-enthalpy and enthalpy-chloride mixing models suggest a reservoir temperature of 124–190°C for the Kizilcahamam region, and a maximum of 71% deep, hot component for the thermal waters (Gulec, 1994).

1.3 Production, temperature and pressure analysis

Figures 5 through 7 give the cumulative production and re-injection, temperature and average dynamic level histories for each well. As can be seen from these figures, well MTA-1 was used as a production well until July 1998 and as a re-injection well starting in the winter of 1998. During summers, only MTA-2 operated, explaining the flat production observed for the other wells.

The total production to re-injection ratio was found to be 3.2. This ratio is relatively high for a low temperature geothermal field, indicating that pressure decline is greater than it should be. An example of this can be seen in Figure 7. Therefore, this ratio must be reduced for good pressure support and efficient management of the field. A good value for this ratio is about 1.5

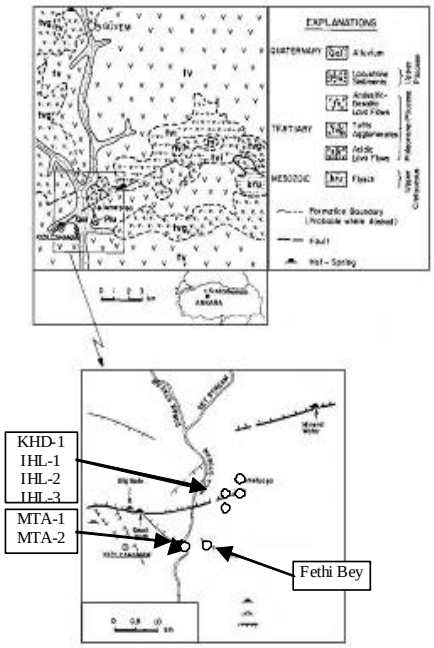

Figure 2: (A) Geological map of Kızılcahamam area (Erol, 1955), (B) Location of wells in Kızılcahamam Geothermal Field (Revised from Özbek, 1988).

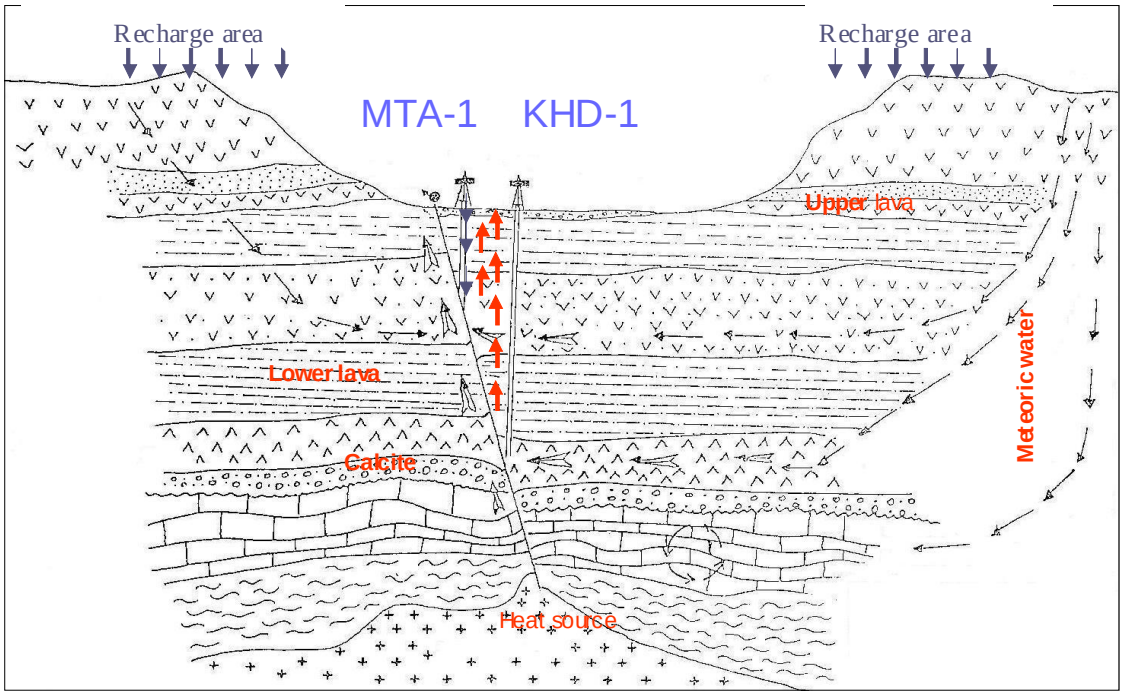

Figure 3: Conceptual model of Kizilcahamam geothermal field.

Temperature measurements of the wells are given in Figure 6. The MTA-1 well was used as a production well until July 1998 and as a reinjection well afterward. The well head temperature was 75-80°C before re-injection started but dropped to 42°C after re-injection. It can be observed that the temperature increased when a well was shut-in during summer.

The temperature of the field does not seem to be affected by re-injection with the exception of IHL-1. Since, IHL-1 is a production well that is not near to a re-injection well, such temperature drops are not expected. This drop may result from cold freshwater intrusion into the well possibly due to mechanical failure such as that of a cement bond or casing or liner failure

.

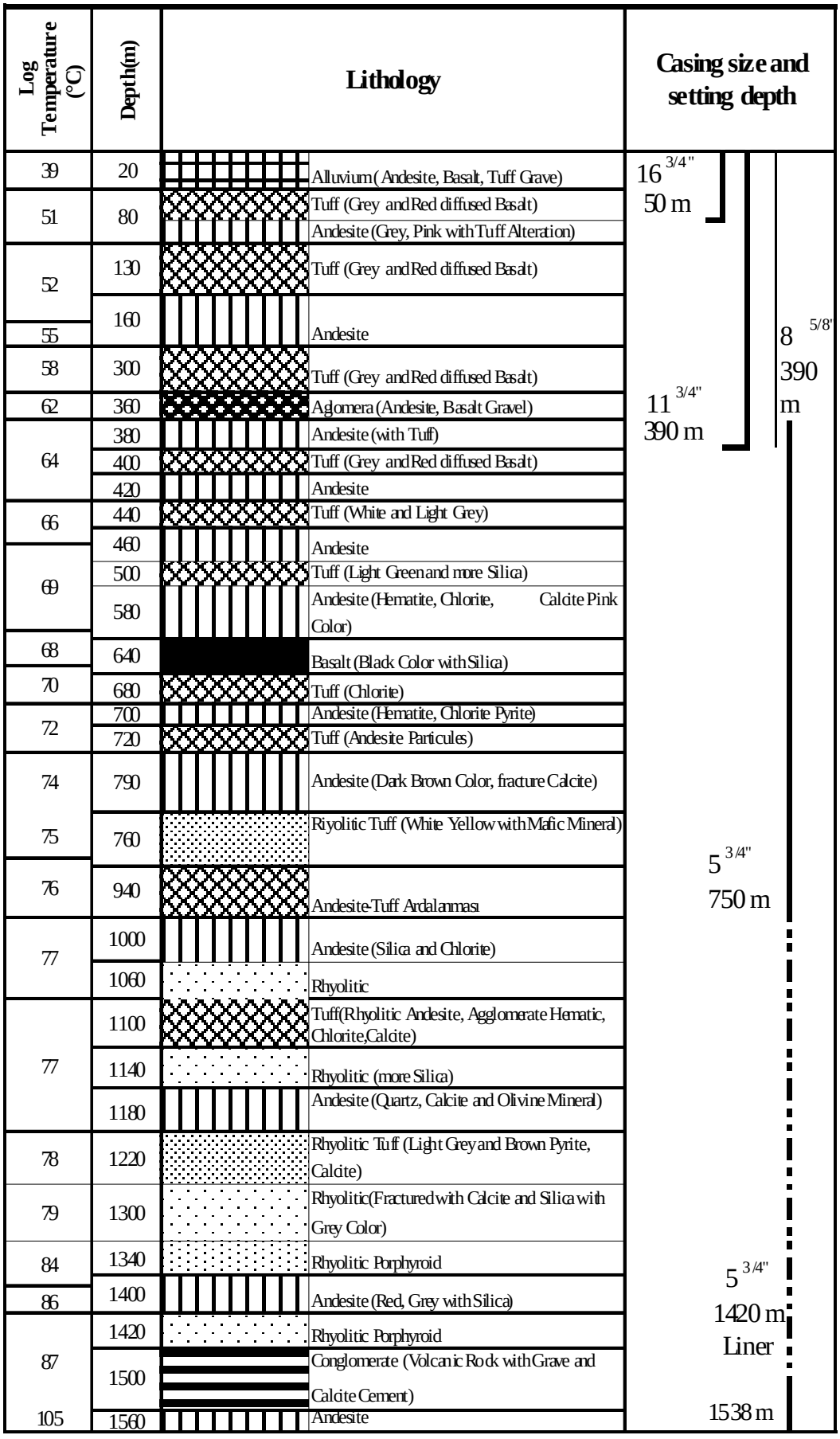

Figure 4: Stratigraphic column of well KHD-1, Kizilcahamam Geothermal Field (Kaya, 2005)

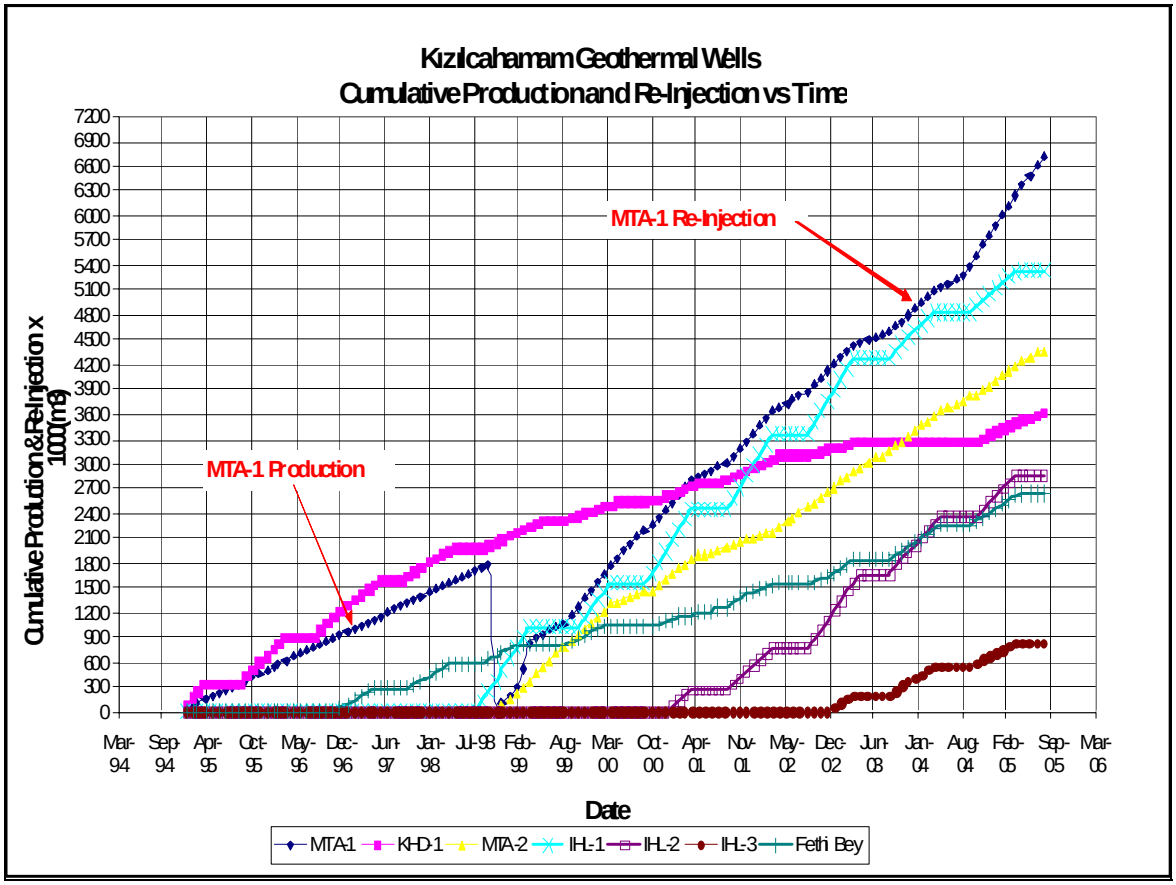

Figure 5: **Production and re-injection history of wells in Kizilcahamam Geothermal Field (Kaya, 2005)**

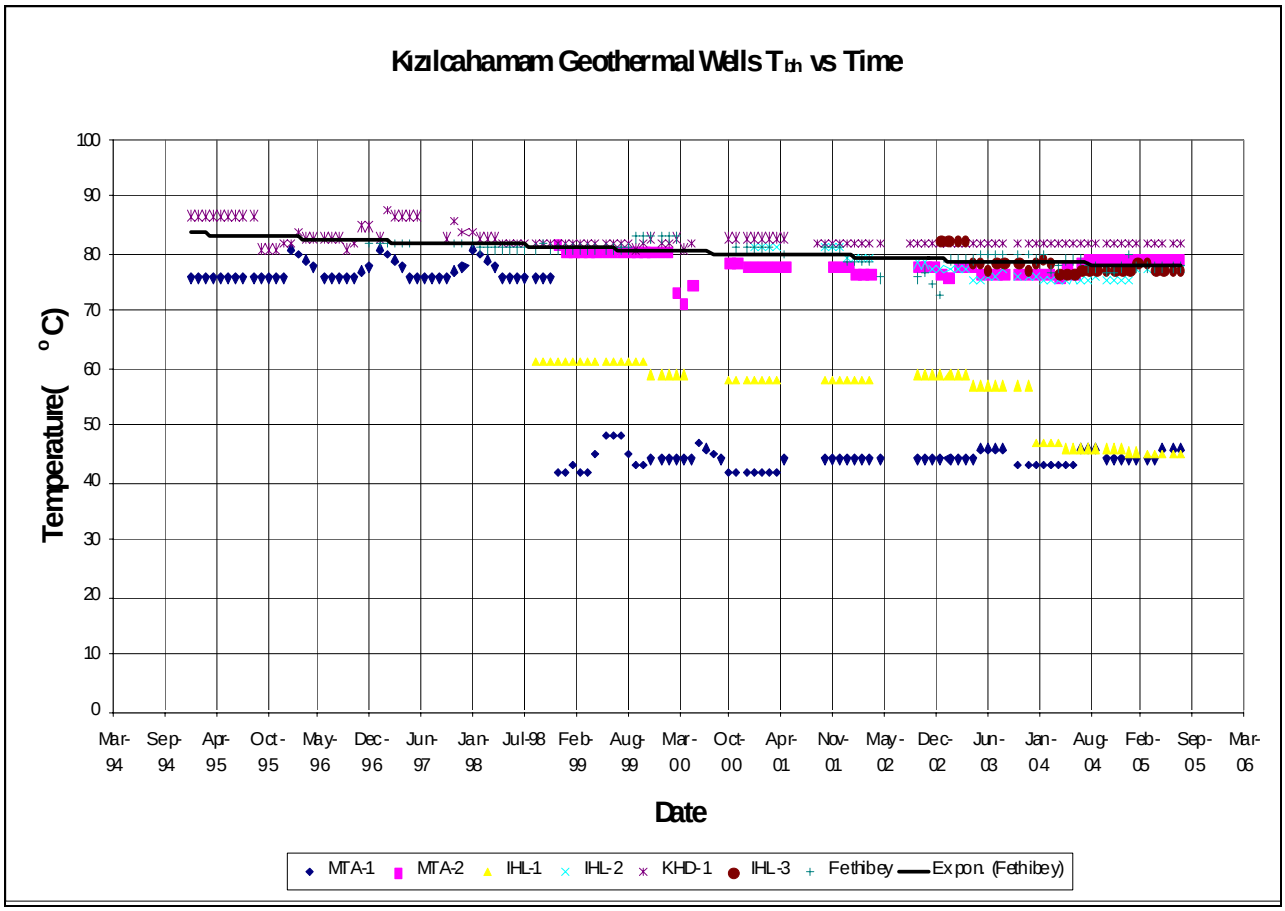

Figure 6: **Temperature history of wells in Kizilcahamam Geothermal Field (Kaya, 2005)**

Pressure declines observed in the field (shown in Figure 7) suggest that in 2011, the pump setting depths must be increased. Yet another strategy to maintain the dynamic levels is to decrease the total production to re-injection ratio. A final solution is the change of re-injection location for better pressure support

2. TRACER TEST DESIGN

In order to determine the amount of fluoreiscein to inject into the reservoir, a literature survey was conducted, and 33 design methods were determined. Most of the methods are empirical equations that depend on the chemicals used in the tracer test, the type of formation to be injected into (karst, sandstone, etc.), the existence of fractures, and the permeability of the formation. In these methods, the main aim is to determine the amounts of the chemicals used in injection fluid. For example, Kilpatrick (1993) offered to use M (mass) = V (volume) / 200 in order to determine the mass of the tracer. Field (2003) observed that most design methods are applicable for only one chemical (like fluorescein) or one formation type (i.e, fractured, karstic, etc). The design equations are usually functions of flow rate, distance between wells, and time.

The most complex part of a tracer test is the determination of the sampling frequency in the investigation well. To determine the sampling frequency two basic methods are offered. Methods that depend on the samples of the tracer tests have sampling frequencies of hours, days and weeks (at most 1-2 weeks). Methods calculated by using the travel distance and time of the tracer chemical. It was reported in different studies that the quantitative methods gave incorrect results. In one quantitative method offered by Kirkpatrick and Wilson (1989), the time of the peak concentration of the tracer is determined using Equation 1:

$$t_p = 2.78x10^{-4}\frac{L}{v_p} \qquad (1)$$

where L is the distance between the wells and v_p is the velocity. The sampling frequency is determined by dividing the test time by 30.

The amount of the chemical and the sampling frequency used in this project was determined by EHTD method offered by Field (2003). This method depends on the solution of Equation 2:

$$R_d\frac{\partial C}{\partial t} = D_z\frac{\partial^2 C}{\partial z^2} - \upsilon\frac{\partial C}{\partial z} - \mu z \qquad (2)$$

where R_d is the dimensionless dissolving factor, C is concentration, t is time, D_z is the axial diffusion constant, υ is the average velocity, and μ is the solvent viscosity. In this equation, it is assumed that the tracer is injected as a slug and no reaction takes place. For the other boundary conditions such as continuous injection, Field (2003) offered different solutions, as shown in Equation 3:

$$f(x^*) = C_p - \frac{M}{An_e\sqrt{4\pi D_z t_p}} \qquad (3)$$

In order to use this equation, the mass of the tracer chemical *M*, flow rate *Q*, porosity n_e, axial dispersivity D_z, area *A*, and the peak concentration time t_p, should be known. Field used the functional dependence of these parameters on flow rate and travel time in order to determine the tracer concentration, tracer mass and axial dispersivity using the Continuous Stirred Tank Reactor (CSTR) model. For the unknown parameters, correlations were used.

Using the EHTD method, it was determined that 1.53 kg of the tracer was required for injection. The following assumptions were made in this calculation: a *fluoreiscein* flow rate of 40 l/s (into re-injection well MTA – 1), a 50 m reservoir formation thickness, a reservoir porosity of 8.0%, and a well separation of 100 m.

It was also assumed that the tracer would be injected for 4 hours. The expected values of chemical concentration and sampling frequency (circles) are shown in Figure 8.

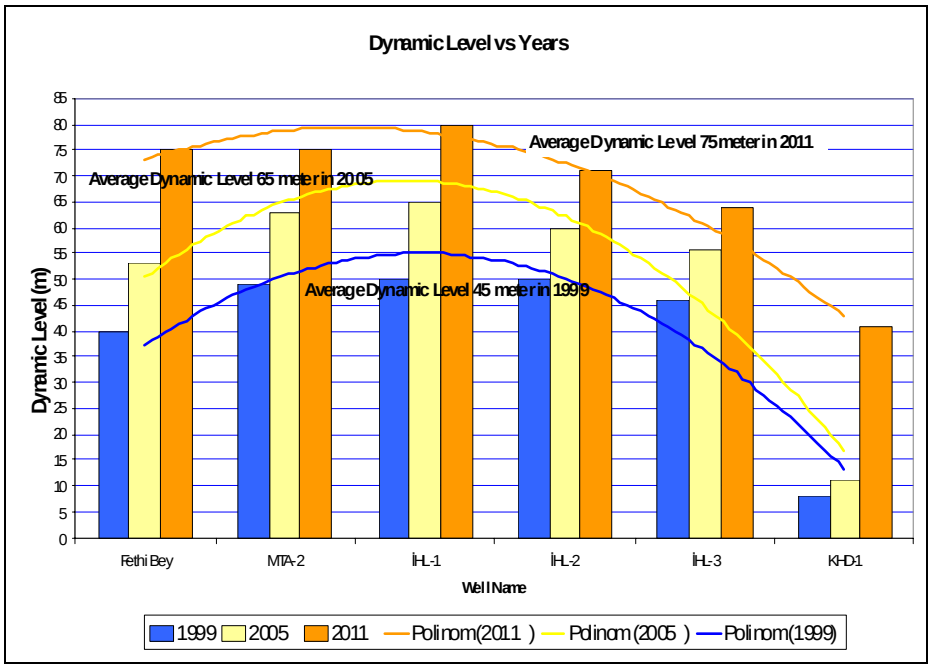

Figure 7 Pressure profile of wells in Kizilcahamam Geothermal Field at different times (Kaya, 2005)

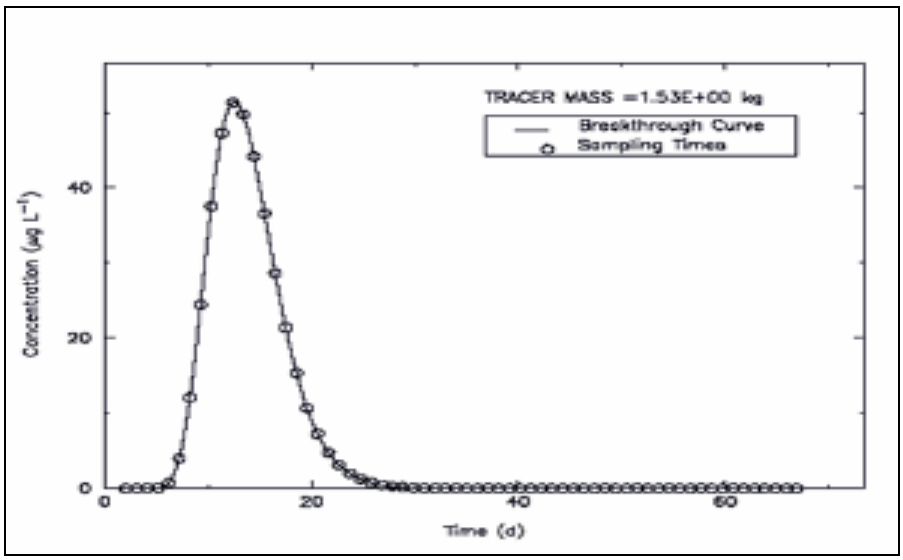

Figure 8: **The expected values of chemical concentration and sampling frequency**

2.1 Implementation of tracer test

The flow rate, temperature and dynamic level measurements were taken in the production and re-injection wells. Flow rates were measured using a Danfoss 3000 magnetic flow meter, temperatures were measured using a thermometer, and static and dynamic levels in production wells were measured using nitrogen injection lines. The wellhead of MTA-1 well was modified for the tracer test. All production well heads were prepared for sample collection purposes. Using ½" and 1" valves after pump discharged head before the control valves. 1.53 kg of fluorescein was mixed with 20 kg water and then injected into well MTA-1 in nearly 6 minutes. Prior to the tracer test, calibration samples were collected from each well. After that, samples were collected in 0.5 liter sample bottles. The fluorescein concentration was detected using a Turner Quantech Fluorimeter. Samples were placed in 3.5 ml Suprasil quartz cuvettes and a 490 nm narrow band excitation filter was used in measurements. First, a calibration fluid was prepared for different concentrations (i.e. 1, 2, 4, 8, 10, 20, 30, 40 and 50 ppb). Following that, a calibration run was conducted. A regression constant larger than 0.9 was used in all measurements. Next, samples were placed in round 3.5 ml cuvettes, and measurements were conducted. Calibration was repeated each day, as the fluorimeter required re-calibration once the device was turned off.

2.1 Tracer Analysis

2.1.1 Tracer Models

Experimental tracer data was analyzed using the multi-fracture, single fracture, uniform porous (1-D and 2-D), fracture-matrix, double porosity pseudo steady state, double porosity cubes, and double porosity slabs models (Akin, 2001). The models were matched to field data using non-linear least-squares approximation. Microsoft Excel Solver uses the Generalized Reduced Gradient (GRG2) nonlinear optimization code developed by Lasdon and Waren (Fylstra et al. 1998). By minimizing the objective function R shown in Equation 4, the parameters of the proposed analytical transfer functions can be estimated.

$$R = \sum_{i=1}^{n} w_i (C_{\mathrm{mod}\,el} - C_{\mathrm{exp}\,eriment})^2 \qquad (4)$$

Here, w_i is the inverse of the variance of the experimental measurement error, which give the maximum-likelihood/minimum-variance estimates of the parameters (Akin, 2001).

The flow of tracer between an injection and production well pair has been described both analytically and numerically by a number of authors. In this study, six different models were considered: multi-fracture model, fracture-matrix model, uniform porous model, double porosity slabs model, double porosity cubes model, and double porosity pseudo steady state model. In each model, it is assumed that there is a good connection between the injection and production wells along a streamline, which is surrounded by a stream tube of constant cross section. The tracer is injected as a slug from the injection well and the response is recorded in the observation well (Akin, 2001). The description of each model is given below.

2.2.2 Multi-Fracture Model

This model, as reported by Fossum and Horne (1982), assumes a single/multi fracture system, joining the injection and observation wells. Dispersion is due to the high velocity profile across the fracture and molecular diffusion, which moves tracer particles between streamlines (Taylor dispersion). The transfer function C_t is given in Equation 5:

$$C_t = \sum_{i=1}^{n} e_i C_r (R_i / u_i, P_{ei}) \qquad (5)$$

Here, n is number of flow channels in the fracture system, e_i is the flow contribution coefficient, R_i is the apparent fracture length, u_i is the velocity, and P_{ei} is the Peclet number of the i^{th} flow channel. Therefore, if "n" is taken as one then only a single fracture is present. It should be noted that for all practical purposes, a multi fracture system must be represented by at least two fractures, since the value of transfer function C_t, does not change much as "n" increases (Akin, 2001).

The form of C_r for each of the paths with a tracer mass concentrated at point x=0 at time=0 is given in Equation 6:

$$C_r = L\frac{1}{\sqrt{t}}\frac{2t_m}{t}Exp\left(\frac{-P_e(t-t_m)^2}{4t_m t}\right) \quad (6)$$

Here, P_e is a Peclet number corresponding to the ratio of tracer transport by advection to tracer transport by diffusion, t_m is the mean arrival time (seconds), and L is a model parameter. Using the above model and by knowing the distance between the injector and producer (R), it is possible to obtain m, the mass of tracer entering the stream tube. The dispersion coefficient for each flow channel can be calculated using the definition given in Equation 7:

$$D_{tr} = \frac{R^2}{P_e t_m} \quad (7)$$

It should be noted that the above model could also be used together with other models.

2.2.3 Fracture-Matrix Model

In this model, as reported by Bullivant and O'Sullivan (1989), there is a large fracture with micro fracturing in the rock matrix on either side. Tracer particles leave the main fracture and enter the micro fracture network (there is a small amount of fluid exchange), stay for a while, and then return to the main fracture.

Longitudinal dispersion due to the velocity profile across the fracture is ignored in order to give a clear distinction from the single fracture model. In this model, it is assumed that the fracture has constant fluid velocity across its thickness and that diffusion is perpendicular to the fracture into an infinite porous medium. The solution is given in Equation 8:

$$C_r = JU(t-t_b)^{-1/2}Exp\frac{-t_b}{w(t-t_b)} \quad (8)$$

Here U is the Heaviside step distribution, w is the ratio of transport along the fracture to transport out of the fracture, t_b is the response start time, and J is a model parameter.

2.2.4 Uniform Porous Model

In the uniform, homogeneous porous model, it is assumed that a slug of tracer is instantaneously injected into a system with constant thickness. It is also assumed that the flow is rapid, allowing the kinematic dispersion components to be predominant. For purely hydrodispersive transfer, the solution for one-dimensional flow as reported by Sauty (1980) is given in Equation 9:

$$C_r = \frac{K}{\sqrt{t_r}}Exp(-\frac{P_e}{4t_r}(1-t_r)^2) \quad (9)$$

where

$$K = \sqrt{t_{rm}}Exp(\frac{P_e}{4t_{rm}}(1-t_{rm})^2) \quad (10)$$

$$t_{rm} = \sqrt{1+P_e^{-2}} - P_e^{-1} \quad (11)$$

In the above equations, P_e is the dimensionless Peclet number, t_r is the mean arrival time, and K is a model parameter. Similarly, Sauty (1980) also reported an analytical expression for the slug injection of a tracer solution into a two dimensional field. The solution of the flow axis can be obtained similarly to the one-dimensional form, as shown in Equation 12:

$$C_r = \frac{K}{t_r}Exp(-\frac{P_e}{4t_r}(1-t_r)^2) \quad (12)$$

where

$$K = t_{rm}Exp(\frac{P_e}{4t_{rm}}(1-t_{rm})^2) \quad (13)$$

$$t_{rm} = \sqrt{1+4P_e^{-2}} - 2P_e^{-1} \quad (14)$$

2.2.5 Double Porosity Slabs Model

The double-porosity slabs model has parallel fractures with constant thickness (a) separated by slabs of the rock matrix giving a constant separation (b) (Bullivant and O'Sullivan, 1989).

Tracer movement in slabs is modeled by diffusion perpendicular to the fractures. If the ratio of transport along the fracture to transport out of the fracture w, the response start time t_b, the matrix block fill up time t_f, the model parameter J, and the injection rate Q are known, the mass of tracer m and the ratio of fracture porosity ϕ_f to matrix porosity ϕ_m can be estimated using Equation 15:

$$C_r = JExp(-t_b(2\sqrt{\frac{p}{wt_b}}\tanh(\frac{t_f}{2}\sqrt{\frac{p}{wt_b}}) + p)) \quad (15)$$

Here, p is the Laplace transform parameter.

2.2.6 Double Porosity Cubes Model

In the double-porosity cubes model as reported by Bullivant and O'Sullivan (1989), it is assumed that the rock matrix consists of cubic blocks of side length b separated by high permeability fractures of aperture a.

The double-porosity cubes model differs from the double-porosity slabs model because for the cubes model, the area of the surface a distance b/2+z from the nearest fracture is proportional to the square of z, whereas for the slabs model the area of the surface a distance b/2-z from the nearest fracture does not vary with z. This affects the way tracer diffuses into the block. Tracer movement in the blocks is modeled by diffusion perpendicular to the nearest face. The solution is given by Equation 16:

$$C_r = JExp(-t_b(2\sqrt{\frac{p}{wt_b}}\coth(\frac{t_f}{2}\sqrt{\frac{p}{wt_b}}) - \frac{4}{t_f} + p)) \quad (16)$$

2.2.7 Double Porosity Pseudo Steady State Model

For this model, the reservoir contains uniformly distributed high permeability microfractures which divide the reservoir into low permeability blocks that consist of pores unswept by fluid flow.

Similarly to the mechanism defined for the fracture-matrix model, the tracer leaves the micro fractures and then returns again. However, the effect is different, such that the blocks

may be filled with tracer. Longitudinal dispersion due to the movement of fluid into the microfracture network is neglected. The solution for this case is reported by Bullivant and O'Sullivan (1989) and given in Equation 17:

$$C_r = J\exp(-\alpha_m t)U(t-t_b)^{1/2} I_1(2(t_b\alpha_f\alpha_m(t-t_b))^{1/2}) \quad (17)$$

Here, α_m is matrix porosity, α_f is fracture velocity, af is the rate of tracer interchange per unit fracture volume, and αm is the rate of tracer interchange per unit matrix volume.

2.2.8 First Temporal Moments

Tracer tests have also been analyzed by Shook (2003) [18] using first temporal moments method. In this method, the flow-storage capacity curve is obtained by conducting a moment analysis of the tracer concentration curves. First, the slope of the tracer curve is taken. Then, the ratio of the flow capacity in each fracture to the flow capacity of the entire fracture network is calculated. After calculating the storage capacity using Equation 20, the flow capacity is obtained as a function of the storage capacity using Equations 20 and 21.

$$f_i = \frac{k_i A_i / L_i}{\sum_{j=1}^{N} k_j A_j / L_j} \quad (18)$$

$$c_i = \frac{V_{pi}}{\sum_{j=1}^{N} V_{pj}} \quad (19)$$

$$F_i = F_{i-1} + f_i \quad (20)$$

$$C_i = C_{i-1} + c_i \quad (21)$$

3. RESULTS AND DISCUSSIONS

Tracer concentration time plots were analyzed using the aforementioned mathematical models. Residual sum of squares values were used to identify the best matching model for the tracer return curves reported for the Fethibey and MTA-2 wells, which are shown in Figures 9 and 10.

These results show that the Kızılcahamam field is not a homogeneous field that can be represented using simple homogeneous models such as uniform porous models or the single fracture model. The results of the tracer analyses are reported in Tables 2 and 3 for each virtual fracture.

The aforementioned findings were verified using moment analysis, as shown in Figures 11-13. As the flow – storage capacity curve deviates from the 45° line, the reservoir section around the corresponding well becomes more heterogeneous. As shown in the flow-storage capacity curves, the fracture system around MTA-2 is more heterogeneous than that of Fethibey. In the region between the injection well MTA-1 and production well FethiBey, 40% of the flow is supplied from 23% of the reservoir. On the other hand, in the region between MTA-1and MTA–2, 40% of the flow is supplied by 11% of the reservoir. The derivative of a flow – capacity curve gives the interstitial velocity (Wu et al 2008). In particular, fracture velocities are faster than the average velocity around MTA-2, but they are slower than the average around Fethibey region. Around MTA-2, flow velocities are 2–3 times faster than those in the Fethibey region. The reinjection area represented in Figure 13 is more heterogeneous, and the existence of multiple flow systems is shown by inflection points on the interstitial velocity plot. This shows that there are at least 3 major flow systems around the injection well.

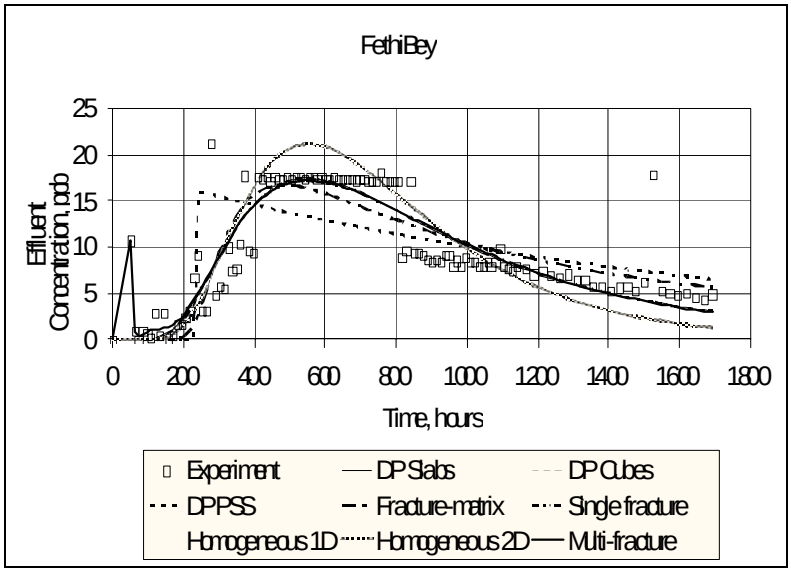

Figure 9: Comparison of Fethibey tracer data to curves of each model.

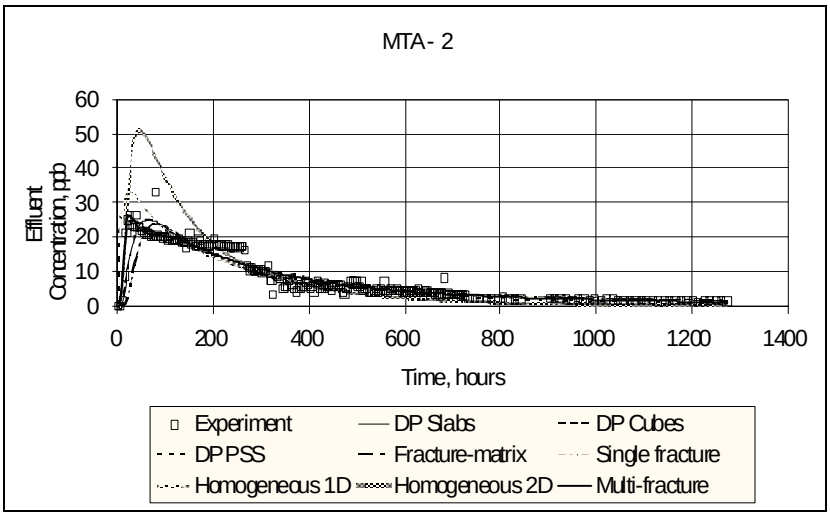

Figure 10: Comparison of MTA-2 tracer data to curves of each model.

Table 2: Fethi Bey tracer matching parameters

Peclet number	Fracture Length(m)	Mean arrival time (hrs)	% contribution	D_l, dispersion m^2	U, m/hrs
70.61	7425.20	40.33	0.01	56.19	9.92
5.44	968.97	932.70	0.18	31.52	0.43
15.20	6.11	146.92	0.81	71.64	2.72
				Apparent velocity	**4.36**

Table 3: **MTA-2 tracer matching parameters**

Peclet number	Fracture Length(m)	Mean arrival time (hrs)	% contribution	D_l, dispersion m^2	U, m/hrs
50.92	0.41	46.24	0.07	0.38	0.65
1.44	529.47	624.59	0.10	1.00	0.05
1.77	49.73	89.93	0.83	5.66	0.33
				Apparent velocity	**0.35**

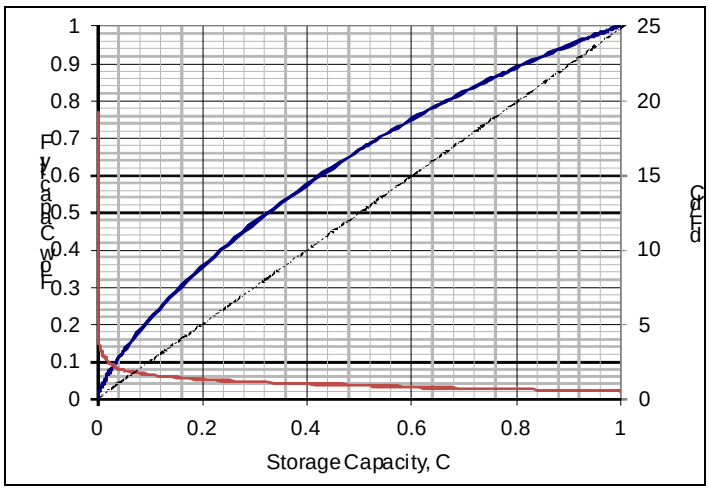

Figure 11 FethiBey tracer test flow-storage capacity curve.

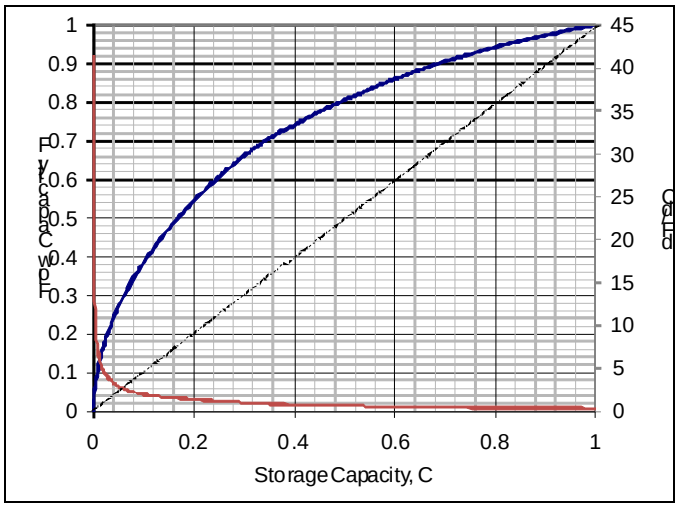

Figure 12 MTA-2 tracer test flow-storage capacity curve.

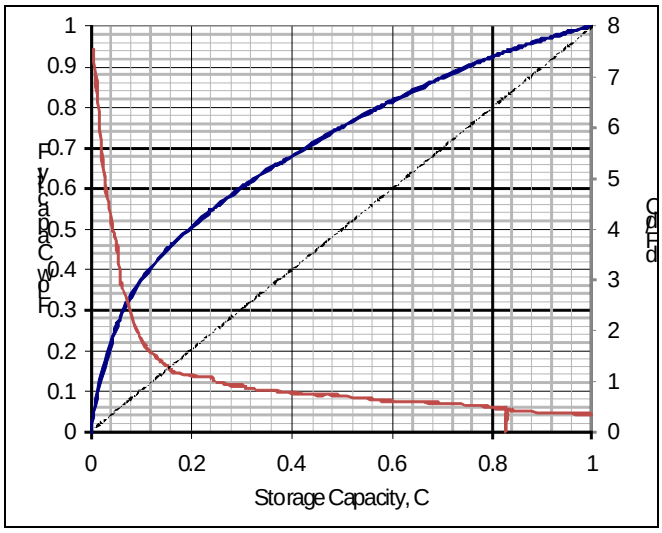

Figure 13 MTA-1 tracer test flow-storage capacity curve.

4. CONCLUSIONS

1. The largest temperature drop since re-injection in MTA-1 was observed in IHL-1. However, it is believed that a cold water zone encroachment is responsible due to cement failure or mechanical problems (casing failure) in the wellbore.
2. Although a re-injection scheme was applied in the Kızılcahamam geothermal field, a decline in pressure was still observed, while the temperature drop was insignificant.
3. Total production to re-injection ratio was found to be 3.2. This ratio is relatively high for a low temperature geothermal field, and this shows that pressure decline is more than it should be.
4. The interpretation of the tracer test shows that there is communication between re-injection well MTA-1 and other wells in the field.
5. A multi-fracture tracer model with three fractures was found to be the most suitable model to describe the Kızılcahamam low temperature geothermal field.
6. The Kızılcahamam field is not a homogeneous field that can be represented using simple homogeneous models such as uniform porous models or the single fracture model.
7. In the region between the wells MTA-1 and FethiBey, 40% of the flow was supplied by 23% of the reservoir. On the other hand, in the region between MTA-1 MTA–2, 40% of the flow was supplied by 11% of the reservoir.

REFERENCES

Akin, S.: Analysis of Tracer Tests with Simple Spreadsheet Models, 2001, *Computers & Geosciences*, 27, 2, 171-178.

Bullivant, D.P., O'Sullivan, M.J.: Matching a field tracer test with some simple models, 1989, *Water Resources Research* 25 (8), 1879±1891.

Demirorer, M.: Ankara-Kızılcahamam rezistivite etudu", in Turkish, 1985, *MTA Report No. 7781*.

Erol, O.: Koroglu Isıkdaglari volkanik kutlesinin orta bolumleri ile Beypazari-Ayas arasindaki Neojen havzasinin jeolojisi hakkinda rapor (in Turkish), 1955, *MTA Report No: 2299.*

Field M. S.: A review of some tracer-test design equations for tracer-mass estimation and sample-collection frequency, 2003, *Environ Geol* 43 (8): 867-881.

Fossum, M.P., Horne, R.N. :Interpretation of tracer return profiles at Wairakei geothermal field using fracture analysis., 1982, *Geothermal Resources Council, Transactions* 6, 261±264.

Fylstra, D., Lasdon, L., Watson, J., Waren, A.: Design and use of the Microsoft Excel Solver., 1998, *Interfaces* 28 (5), 29-55.

Gevrek, A.I.: Water/rock interaction in the Kizilcahamam Geothermal Field, Galatian Volcanic Province (Turkey): a modelling study of a geothermal system for re-injection well locations, 2000, *Journal of Volcanology and Geothermal Research*, 96 (3-4), 207-213.

Gevrek, A.I., Aydin, S.N: Hydrothermal alteration studies in Kızılcahamam Ankara geothermal field and its evolution on the development of this field., 1988, *In: Proc. Int. Mediterranean Congress on Solar and Other New-Renewable Energy Resources,* 14–19 Nov., Antalya. pp. 609–616.

Gulec, N: Geochemistry of thermal waters and its relation to the volcanism in the Kizilcahamam (Ankara) area, Turkey, 1994, *Journal of Volcanology and Geothermal Research*, 59, 4, 295-312.

Gurer, A., Celik, I.: Kızılcahamam ve cevresinin sismik etudu" in Turkish, 1987, *MTA Report No. 8766.*

Kaya, T.: Characterization of Kizilcahamam geothermal field by tracer testing", 2005, Msc Thesis, Middle East Technical University.

Kilpatrick ,F. A.: Simulation of Soluble Waste Transport and Buildup in Surface Waters Using Tracers, 1993, *Tech.Rep.Techniques of Water-Resources Investigations*, Book 3, Chapter A20,37 p., U.S. Geological Survey.

Kilpatrick ,F. A., Wilson Jr.,J.F.,: Measurement of Time of Travel in Streams by Dye Tracing., 1989, *Tech. Rep.27 Techniques of Water-Resources Investigations of the U.S. Geological Survey*, Book 3, Chapter A9, 27 p., U.S. Geological Survey.

Kocak, A.: Kızılcahamam kaplicasi hidrojeolojisi etudu" in Turkish, 1977, *MTA Report No. 5669.*

Ongur, T. "Kızılcahamam, Camlidere, Celtikci ve Kazan dolayinin jeolojisi ve jeotermal enerji olanaklari", in Turkish, 1976, *MTA Report No. 5669.*

Ozbek, T.: Interpretation of Ankara-Kizilcahamam geothermal area, 1988, *U.N. Seminar on New Developments in Geothermal Energy*, 22-25 May 1989, Ankara.

Sauty, J.P.: An analysis of hydrodispersive transfer in aquifers, 1980, *Water Resources Research* 16 (1), 145-158.

Tatli, S.: Kızılcahamam dogu alani jeolojisi ve jeotermal enerji olanaklari, in Turkish, 1975, *MTA Report* No. 5749.

Wu, X., Pope, G.A., Shook, M.G., Srinivasan,S.: Prediction of enthalpy production from fractured geothermal reservoirs using partitioning tracers., 2008, *Int J Heat & Mass Trans,* 51 (5-6), 1453-1466.